Deep Reinforcement Learning for Dynamic Power Allocation in Cell-free mmWave Massive MIMO

Yu Zhao[a], Ignas Niemegeers[b] and Sonia Heemstra de Groot[c]
Department of Electrical Engineering, Eindhoven University of Technology, Eindhoven, The Netherlands

Keywords: Cell-free Massive MIMO, Deep Reinforcement Learning, Deep Q-Network, Power Allocation.

Abstract: Numerical optimization has been investigated for decades to solve complex problems in wireless communication systems. This has resulted in many effective methods, e.g., the weighted minimum mean square error (WMMSE) algorithm. However, these methods often incur a high computational cost, making their application to time-constrained problems difficult. Recently data-driven methods have attracted a lot of attention due to their near-optimal performance with affordable computational cost. Deep reinforcement learning (DRL) is one of the most promising optimization methods for future wireless communication systems. In this paper, we investigate the DRL method, using a deep Q-network (DQN), to allocate the downlink transmission power in cell-free (CF) mmWave massive multiple-input multiple-output (MIMO) systems. We consider the sum spectral efficiency (SE) optimization for systems with mobile user equipment (UEs). The DQN is trained by the rewards of trial-and-error interactions with the environment over time. It takes as input the long-term fading information and it outputs the downlink transmission power values. The numerical results, obtained for a particular 3GPP scenario, show that DQN outperforms WMMSE in terms of sum-SE and has a much lower computational complexity.

1 INTRODUCTION

Massive multiple-input multiple-output (MIMO) (Larsson and Edfors, 2014) and the use of mmWave spectrum, have been widely recognized as key to increasing the system capacity by an order of magnitude compared to present sub-6 GHz networks (Busari and Huq, 2018). This is because of the larger bandwidth available in the mmWave spectrum and the significantly higher spectral efficiency (SE) that can be achieved with massive MIMO (Andrews and G., 2014).

In massive-MIMO, a base station (BS), equipped with a very large antenna array, serves simultaneously multiple user-equipments (UEs), using the same time-frequency resource. The number of antennas should significantly exceed the number of UEs. Further gains can be obtained by spreading the antennas over multiple geographically distributed access points (APs), instead of concentrating them in a single BS. This leads to the concept of cell-free (CF) massive MIMO, introduced in (Q and Ashikhmin, 2017). The APs jointly and coherently provide service to the UEs. CF massive MIMO still has the benefits of centralized massive MIMO, e.g., favorable propagation and channel hardening, provided there are multiple (e.g., 5 to 10) antennas at each AP (Chen and Björnson, 2018). Favorable propagation means that the UE's channel vectors are almost orthogonal. Channel hardening means that the beamforming transforms the fading multi-antenna channel into an almost deterministic scalar channel. These properties simplify the signal processing and resource allocation. The additional advantages of such an architecture, compared to centralized massive MIMO are that (1) because the antennas are geographically distributed, transmissions are less affected by shadow fading and (2) the average distance from a UE to its nearest AP is smaller. The drawback is the need for an optical or wireless fronthaul to connect the APs with a central controller (CC), see Fig.1.

Since the sub-6 GHz radio spectrum is highly congested, mmWave massive MIMO systems have increasingly attracted attention (González-Coma and Rodríguez-Fernández, 2018; Yu and Shen, 2016; Alonzo and Buzzi, 2019). However, the operation in the mmWave domain poses different and new challenges for CF massive MIMO systems:

[a] https://orcid.org/0000-0002-5639-4470
[b] https://orcid.org/0000-0002-2560-4746
[c] https://orcid.org/0000-0003-2270-727X

Zhao, Y., Niemegeers, I. and Heemstra de Groot, S.
Deep Reinforcement Learning for Dynamic Power Allocation in Cell-free mmWave Massive MIMO.
DOI: 10.5220/0010617300330045
In *Proceedings of the 18th International Conference on Wireless Networks and Mobile Systems (WINSYS 2021)*, pages 33-45
ISBN: 978-989-758-529-6

(1) The full benefit of massive MIMO is obtained by providing each antenna with its own RF chain, which includes the DACs, mixers, etc. (I and H, 2018); this is called full-digital beamforming. Hardware constraints prevent the realization of full-digital beamforming at mmWave frequencies (Alkhateeb and Mo, 2014). Thermal problems, due to the density of the hardware components and the high cost of RF chains, make full-digital beamforming, for the time being, an uneconomical solution. Therefore, one resorts to the more practical hybrid beamforming, which has much less RF chains, that each drive an analog beamforming antenna array (Alkhateeb and Mo, 2014). This, however, degrades the system performance in terms of achievable SE. Several studies, e.g., (O. and S., 2014; F and W., 2016; Lin and Cong, 2019), addressed techniques to decrease this degradation.

(2) Power allocation is another challenge in CF mmWave massive MIMO systems (Alonzo and Buzzi, 2019). Because different UEs are simultaneously served by the same time-frequency block, controlling the inter-UE interference is important. In principle, the suppression of the inter-UE interference could be achieved by using zero-forcing (ZF) beamforming. However, due to the geographical spreading of the antennas, this is not feasible. The ZF algorithm would require the channel state information (CSI) for each channel in the network to be available at the CC, implying an unaffordable control message overhead between APs and the CC and the associated timing issues. Therefore, the conjugate beamforming (CB) or normalized CB (NCB) (Polegre and Palou, 2020), which can be processed locally in APs, are used in CF massive MIMO. Because the inter-UE interference cannot be suppressed by CB or NCB, power allocation is the key to optimize the downlink performance in terms of SE (Björnson and Hoydis, 2017; Hamdi and Driouch, 2016). In this paper we focus on the problem of power allocation to maximize the downlink sum-SE, which requires the solution of a non-convex optimization problem.

Although many existing heuristic algorithms have shown excellent performance for solving non-convex problems, their application in real systems faces serious obstacles because of their computational complexity (Sun and Chen, 2018). For example, the popular weighted minimum mean square error (WMMSE) algorithm requires complex operations such as matrix inversion and bisection in each iteration (Shi and Razaviyayn, 2011). Even when the power allocation is performed at the CC and is done on the large-scale fading time scale (milliseconds for mmWave) (Q and Ashikhmin, 2017), it is still challenging to make an implementation that meets the real-time constraints.

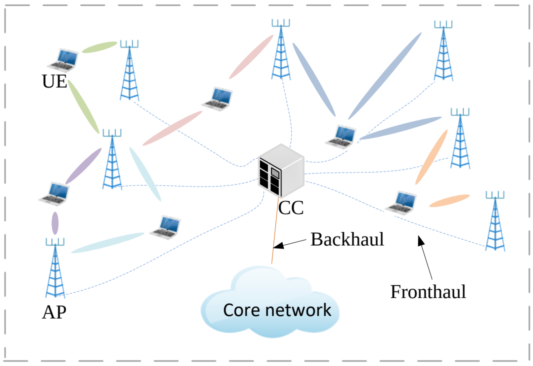

Figure 1: Cell-free massive MIMO system.

Recently deep-learning (DL) data-driven approaches have been tried for power allocation in wireless communication systems, achieving near-optimal performance with affordable computational cost, e.g., (Sun and Chen, 2018) and (Chien and Canh, 2020; Nikbakht and Jonsson, 2019; Nasir and Guo, 2019; Meng and Chen, 2020). There are three main branches of DL, namely supervised learning, unsupervised learning, and deep reinforcement learning (DRL). DRL is characterized by how agents ought to take actions in an environment such that the cumulative reward is maximized (Mnih and Kavukcuoglu, 2013). DRL has been applied to solve power optimization problems in non-massive-MIMO cellular networks, e.g., (Nasir and Guo, 2019) used a four-layer DQN and (Meng and Chen, 2020) a five-layer DQN for different network configurations.

In this paper we propose a DRL method to optimize the power allocation in CF mmWave massive MIMO. The reason is that it has a low computational complexity, which, as we will see, is needed to meet certain real-time constraints. Unlike supervised learning, which requires a huge training dataset generated by a computationally complex algorithm, DRL is trained by the rewards of trial-and-error interactions with its environment over time. It requires only a small number (e.g., 4 in our case) of matrix multiplications to perform the power allocation. Moreover, we will show that its performance, in terms of the downlink sum-SE it achieves, is competitive compared with the WMMSE algorithm.

We consider a CF mmWave massive MIMO system that serves several mobile UEs. The objective function of the power allocation is the downlink sum-SE. We assume NCB because it can be performed locally at each AP, which implies that there is no overhead for sending CSI from the APs to the CC via the fronthaul. In addition, NCB can be easily implemented in a hybrid beamforming architecture, since in each RF chain only a phase-shift of the data signal is required in each antenna path (Interdonato and Ngo, 2016). The analysis is carried out using Monte Carlo simulations for a 3GPP indoor mixed-office scenario (3GPP, 2018) with the well-adopted extended Saleh-Valenzuela (S-V) channel model to describe the mmWave propagation (C and K, 2013). Imperfect CSI and pilot contamination are considered in our analysis. The main contributions of this paper are:

1. A closed-form formalization of the downlink sum-SE maximization problem for CF mmWave massive MIMO with multi-antenna APs and single-antenna UEs, taking into account imperfect CSI and pilot contamination.

2. A DRL-based power allocation method, using a deep Q-network (DQN). The inputs to the DQN are the normalized large-scale fading between transmitters and receivers, and the outputs are the downlink transmission powers.

3. An evaluation of the downlink sum-SE obtained by DRL-based power allocation, comparing it with the WMMSE algorithm for a 3GPP indoor mixed office scenario with mobile UEs. The simulation results show that DRL outperforms WMMSE in terms of downlink sum-SE and has a much lower computational complexity.

The rest of the paper is structured as follows. Section 2 describes the system models and power allocation problem. Section 3 describes the DRL based power allocation. Section 4 shows the simulation results and their interpretation. Finally, Section 5 draws the conclusions.

2 SYSTEM MODEL

Consider a CF mmWave massive MIMO system where N APs serve K UEs. Each AP has M antennas, whereas each UE has a single antenna ($K << MN$). All APs are connected to a CC through a fronthaul (Fig.1). We assume the system is driven by $N_{RF} = K$ RF chains to enable K UEs being served simultaneously by the same time-frequency resource block. We do not address the possible limitations the fronthaul links may introduce. As discussed in (Q and Ashikhmin, 2017), these limitations degrade the system performance in terms of achievable SE and should be quantified in further studies. We assume the system operates in TDD mode and the uplink and downlink channels are reciprocal. We focus on the downlink.

Typically, the length of the time-frequency resource block is chosen to be the coherence time τ_c, i.e., the time during which small-scale fading has an insignificant effect on the signals. The time-interval of a time-frequency resource block, is divided in two phases: the uplink channel estimation phase and the downlink data transmission phase. During the uplink channel estimation, the UEs send pilots to the APs and each AP estimates the corresponding channels. During the downlink data transmission, the estimated channels are used to perform beamforming and transmit the payload data. The duration of the uplink channel estimation phase is denoted by τ_p, where $\tau_p < \tau_c$ and the duration of the downlink data transmission phase is then $\tau_c - \tau_p$. The beamforming, used during the data transmission phase and based on the CSI values collected, will be valid for approximately the coherence time. This implies that there are real-time constraints on the computation of the beamforming: the results should be available before the start of each data transmission phase. If one has the benefit of channel hardening, i.e., small-scale fading can be neglected, due to the spatial diversity created by the large number of antennas (Chen and Björnson, 2018), power allocation can be done on a longer time scale, commensurate with the large-scale time τ_l. τ_l is defined as the time during which the effect of large-scale fading can be considered to be constant. It typically is around 40 times the coherence time τ_c (Q and Ashikhmin, 2017; Mai and Ngo, 2020). Fig.2 shows the time scales for beamforming and power allocation.

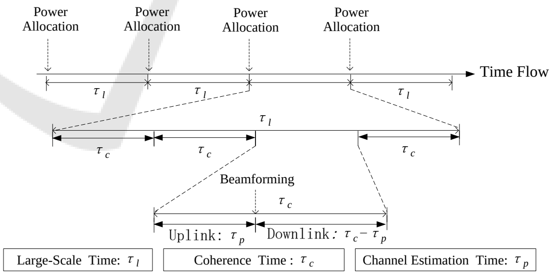

Figure 2: Time scales for beamforming and power allocation.

2.1 Channel Model

We use the extended S-V channel model to describe the propagation of the mmWave signals. One could also choose other channel models such as the IEEE 802.11ad or the IEEE 802.15.3c models, which are similar to the extended S-V model (C and K, 2013). The channel vector from AP n to UE k can be formulated as follows (Busari and Huq, 2018):

$$\mathbf{g}_{n,k} = \sqrt{\frac{M}{L}} \sum_{l=1}^{L} \alpha_l^{n,k} \mathbf{f}_r(\psi_{l,r}^{n,k}, \theta_{l,r}^{n,k}) \mathbf{f}_t^H(\psi_{l,r}^{n,k}, \theta_{l,t}^{n,k}) \quad (1)$$

where L is the number of propagation paths from AP n to UE k, $\alpha_l^{n,k}$ is the pathloss of the l-th path, $\psi_{l,r}^{n,k}$ and $\theta_{l,r}^{n,k}$ are the azimuth and elevation angle of the angle of arrival (AoA) of path l, where subscript r stands for reception, $\psi_{l,t}^{n,k}$ and $\theta_{l,t}^{n,k}$ are the azimuth and elevation angle of the angle of departure (AoD) of path l, where subscript t stands for transmission, and $\mathbf{f}_r(\psi_{l,r}^{n,k}, \theta_{l,r}^{n,k})$ and $\mathbf{f}_t(\psi_{l,t}^{n,k}, \theta_{l,t}^{n,k})$ are the receive and transmit antenna array response vectors with dimensions equal to the number of receive and transmit antennas respectively. The antenna response vectors $\mathbf{f}$ depend on the particular antenna design and array configuration. In our downlink analysis we assume the transmission antenna is a uniform planar array (UPA) with $U_1 \times U_2$ elements. For this case, the response vector $\mathbf{f}_t(\psi_{l,t}^{n,k}, \theta_{l,t}^{n,k})$ has $U_1 \times U_2$ elements and takes the following form (O. and S., 2014):

$$\mathbf{f}_{\text{UPA}}(\psi, \theta) = \frac{1}{\sqrt{U_1 U_2}} [1, \ldots, e^{j2\pi \frac{d}{\lambda}(u_1 \sin(\psi)\sin(\theta) + u_2 \cos(\theta))}, \ldots, e^{j2\pi \frac{d}{\lambda}((U_1-1)\sin(\psi)\sin(\theta) + (U_2-1)\cos(\theta))}]^H \quad (2)$$

where u_1= [1, 2, …, U_1], u_2 = [1, 2, …U_2], d is the antenna spacing and λ is the wavelength. In our case we choose U_1=U_2 = $\sqrt{M}$. Since we assume that all UEs are equipped with a single omnidirectional antenna, the reception response vector $\mathbf{f}_r(\psi_{l,r}^{n,k}, \theta_{l,r}^{n,k})$ in (2), reduces to a scalar with value 1.

2.2 Uplink Channel Estimation

By using the minimum mean-square error (MMSE) estimation (Björnson and Hoydis, 2017), the estimate $\hat{\mathbf{g}}_{n,k}$ includes M i.i.d. Gaussian components. The mean-square of the m-th component is denoted by $\gamma_{n,k}$, given by:

$$\gamma_{n,k} = \frac{\tau_p p_p \beta_{n,k}^2}{\tau_p p_p \sum_{k'=1}^{K} \beta_{n,k'} |\phi_{k'} \phi_k^H|^2 + 1} \quad (3)$$

where p_p is the normalized pilot power, ϕ_k is the pilot sequence transmitted by UE k, $\beta_{n,k}$ represents the large-scale fading between AP n and UE k.

2.3 Downlink Data Transmission and Spectral Efficiency

Based on the estimated channels, the APs employ NCB to transmit signals to UEs. UE k will receive the superposition of the signals of all APs in the whole system:

$$y_k = \sum_{n=1}^{N} \sum_{k'=1}^{K} \sqrt{p_{n,k'}} \frac{\mathbf{g}_{n,k}^T \hat{\mathbf{g}}_{n,k'}^*}{\sqrt{M \gamma_{n,k'}}} q_{k'} + w_k \quad (4)$$

where $p_{n,k'}$ is the normalized downlink transmission power from AP n to user k' satisfying $p_{n,k'} \leq p_{\max}$, $p_{\max}$ is the power transmission limit and $q_{k'}$ is the intended signal to UE k'. $w_k \sim \mathcal{CN}(0,1)$ is the additive noise at UE k. The downlink SE for user k, is given by (6) in the next page (Björnson and Hoydis, 2017).

2.4 Max sum-SE Power Allocation

We use the max sum-SE power allocation policy, which can be formulated as follows:

$$\begin{aligned} &\max_{p_{n,k}} \sum_{k=1}^{K} SE_k \\ &s.t. \;\; p_{n,k} \leq p_{\max}, \forall n, k \end{aligned} \quad (5)$$

This is a non-convex and NP-hard optimization problem, since the computational complexity increases exponentially as N and K increase. A well-adopted method to solve (5) is the WMMSE heuristic, which converts the sum-SE maximization problem to an equivalent minimization problem of the mean square error in the data detection (Shi and Razaviyayn, 2011). Specifically, the algorithm (Algorithm I) works as follows.

From an initial point $\{v_{n,k}^0\}$ satisfying the constraints, the optimal power allocation is obtained by updating $\{v_{n,k}, u_{n,k}, w_{n,k}\}$ in an iterative manner, where $v_{n,k}, u_{n,k}, w_{n,k}$ are optimization variables. The variables $\{v_{n,k}, u_{n,k}, w_{n,k}\}$, for all n, k in iteration I, are updated using (7) (8) and (9), where (9) implies that the variable $v_{n,k}$ should be in the range from 0 to $\sqrt{p_{\max}}$. The details of the WMMSE algorithm in solving (5) are given by Algorithm1. The algorithm stops when the condition $w_{n,k} < \varepsilon$ is fulfilled. The value of ε depends on the convergence behavior of the WMMSE algorithm. Similarly to (Shi and Razaviyayn, 2011) we set $\varepsilon = 0.01$.

The computational complexity mainly lies in steps 3 and 6. The calculation of $\gamma_{n,k}$ has a complexity of O(K). For the denominator of (7) and (9), the complexity is O(NK^2). So for the updating of $p_{n,k}$, the complexity is O(INK^2), where I represents the number of iteration for WMMSE to converge. Finally, the total complexity to update NK links is O(IN^2K^3).

$$SE_k = (1-\frac{\tau_p}{\tau_c})\log_2(1+\frac{M(\sum_{n=1}^{N}\sqrt{p_{n,k}\gamma_{n,k}})^2}{M\sum_{k'\neq k}(\sum_{n=1}^{N}\sqrt{p_{n,k'}\gamma_{n,k'}}\frac{\beta_{n,k}}{\beta_{n,k'}})^2|\phi_k\phi_{k'}^H|^2+\sum_{k'=1}^{K}\sum_{n=1}^{N}p_{n,k'}\beta_{n,k}+1}) \tag{6}$$

$$u_{n,k}^{l} = \frac{\sqrt{M}v_{n,k}^{l-1}\sqrt{\gamma_{n,k}}}{M\sum_{k'=1}^{K}(\sum_{n'=1}^{N}v_{n',k'}^{l-1}\sqrt{\gamma_{n',k'}}\frac{\beta_{n',k}}{\beta_{n',k'}})^2|\phi_k\phi_{k'}^H|^2+\sum_{k'=1}^{K}\sum_{n'=1}^{N}(v_{n',k'}^{l-1})^2\beta_{n',k}+1} \tag{7}$$

$$w_{n,k}^{l} = \frac{1}{1-u_{n,k}^{l-1}\sqrt{M\gamma_{n,k}}v_{n,k}^{l-1}} \tag{8}$$

$$v_{n,k}^{l} = \min(\max(\frac{w_{n,k}^{l}u_{n,k}^{l}\sqrt{M\gamma_{n,k}}}{\sum_{k'=1}^{K}\sum_{n'=1}^{N}w_{n',k'}^{l}(u_{n',k'}^{l})^2M\gamma_{n',k'}},0),\sqrt{p_{max}}) \tag{9}$$

Algorithm 1: Pseudo Code of WMMSE for (5).

```
Initialize $v_{n,k}^0$ such that $(v_{n,k}^0)^2 \leq p_{\max}, \forall k,n$
Set $I = 1$, repeat:
    Update the variables $u_{n,k}^I$ for all $n,k$, by (7).
    Update the variables $w_{n,k}^I$ for all $n,k$, by (8).
    Update the variables $v_{n,k}^I$ for all $n,k$, by (9).
    Set $I = I + 1$.
    Until $w_{n,k}^I < \varepsilon$.
Output: $p_{n,k} = (v_{n,k})^2$
```

3 DQN BASED POWER ALLOCATION

In this section we propose a DQN to perform the power allocation, combining reinforcement learning with a deep neural network (Mnih and Kavukcuoglu, 2013). This method has low computational complexity: it only requires a small number of layers of simple operations such as matrix or vector multiplications (Sun and Chen, 2018).

3.1 Background of DQN

Deep reinforcement learning (or deep Q-learning) is a category of machine learning where an agent learns by interacting with its dynamic environment through a repeated sequence of observations, actions and rewards (Mnih and Kavukcuoglu, 2013). After each action, the agent observes the effect on the environment and receives a reward which depends on the extent to which the observations get closer to a target. The agent maximizes the cumulative reward along the course of interacting with its environment.

Through trial and error, an agent keeps learning, making this technology ideal for dynamic environments that keep changing. The 'deep' in DQN refers to the fact that the neural network has multiple (deep) internal layers.

The deep reinforcement learning is a discrete-time system. At time step t, by observing the state s_t, the agent takes action $a^t \in \boldsymbol{A}$ according to a certain policy π, then gets the reward r^t from the environment and enters the next state s^{t+1}. The policy $\pi(s,a)$ is the probability of taking action a conditioned on the current state s. The experience sequence, defined as $e^t = (s^t, a^t, r^t, s^{t+1})$, describes a single interaction with the environment. The goal of the agent is to select actions that maximize the future cumulative reward:

$$R^t = r^t + \omega r^{t+1} + \omega^2 r^{t+2} + ... \tag{10}$$

where $\omega \in [0,1)$ is a discount factor that trades off the importance of immediate and future rewards. The action-value (also know as Q function) defines the expected reward once action a is taken in state s under policy π:

$$Q^{\pi}(s,a) = \mathbb{E}_{\pi}\{R^t | s^t = s, a^t = a\} \tag{11}$$

The basic idea behind reinforcement learning is to estimate the optimal action-value function by the Bellman equation (N and H, 1989):

$$Q^{*}(s,a) = \mathbb{E}\{r^t + \omega \max_{a'} Q^{*}(s^{t+1},a')|s,a\} \tag{12}$$

where $Q^{*}(s,a)$ represents the action-value of the optimal policy. It is common to use a function approximator to estimate the action-value function, typically a lookup table or a linear function. If this approximator is a DNN, it is called DQN. The DQN is defined as $Q(s,a,\boldsymbol{\xi})$ where $\boldsymbol{\xi}$ represents the parameters (weights between neurons). The DQN is trained to estimate the optimal action-value function, i.e., the vector $\boldsymbol{\xi}$ is updated to estimate $Q^{*}(s,a)$. The agent stores the experiences in a data set $D = \{e^1, e^2, \dots e^t\}$, which is used to train the DQN by the gradient descent algorithm (LeCun and Bengio, 2015). Ideally the training of DQN should use all data in each iteration, however, this is very expensive when the training set is huge. An efficient way is to use a random subset of the training set, called mini batch, to evaluate the gradients in each iteration (M and T., 2014). The loss function of the DQN for a random mini-batch D^t (random sample over D) at time step t is:

$$L(\boldsymbol{\xi}^t) = \sum_{e \in D^t} (r + \omega \max_{a'} Q(s', a', \hat{\boldsymbol{\xi}}) - Q(s, a, \boldsymbol{\xi}^t))^2 \tag{13}$$

where $e = (s, a, r, s')$, $\hat{\boldsymbol{\xi}}$ represents the network parameters to compute the target at time step t, which is only updated every C steps, see details in (Mnih and Kavukcuoglu, 2013). Finally the stochasitc gradient descent algorithm is used to update $\boldsymbol{\xi}$ over the mini-batch D^t.

3.2 DQN Power Allocation

Typically, DQNs are very suitable to solve problems that can be modeled as Markov decision processes, where the goal of the agent is to maximize the cumulative rewards (Mnih and Kavukcuoglu, 2013). The power allocation in CF mmWave massive MIMO, according to the policy formulated in (5), can be seen as such a Markov decision process: the large-scale fading changes according to the mobility of UEs over time, which, in our case, can be modeled as a Markov process (see Section 4). For a non-Markov process, due to the high correlations between the current state and previous several states, the updates of the DQN have large variances, leading to an inefficient training (Mnih and Kavukcuoglu, 2013). How to reduce the variance of the DQN update is an open issue in case of non-Markovian problems.

To use the DQN solving the power allocation problem in CF mmWave massive MIMO, we define the duration of each time step t as the large-scale time in Fig.2. In scenarios with fixed position UEs, the discount factor ω was suggested to be zero (Meng.F and P., 2019). However, in our case, since we consider mobile UEs, we determine ω by trial-and-error, see Section 4.2.

As in (Nasir and Guo, 2019) and (Meng and Chen, 2020), we define for each AP-UE link an agent, thus the power allocation is performed by a multi-agent system, where each agent contains a DQN. The agents interact with the environment to collect data (s^t, a^t, r^t, s^{t+1}) and store it in a dataset at the CC, then by mini-batch sampling the DQN is trained using the gradient descent algorithm, as shown in Fig.3. Since the learning is done off-line, the overhead cost of the data collection does not affect the operational phase. It is unnecessary to have 'real-time' training in off-line learning mode. The training time, however, could be considerable. We also should clarify that for the off-line learning mode, the DQN is trained by a sufficient dataset, the size depends on the convergence of the sum-SE. Once the training is finished, the DQN is used to perform the power allocation. No further training is needed. However, when there are significant changes in the network configuration, e.g., the number of active APs, or in the temporal and spatial traffic characteristics, the DQN should be retrained. When that should happen and what impact it would have on the operation of the system has not been addressed yet and requires further study.

There is a total of NK agents in the whole system. At time step t, each agent (n,k) allocates power from AP n to UE k. One should note that all agents use the same DQN parameters, i.e., after the DQN is trained by the experience of all agents, the DQN shares its parameters with all other agents to allocate power.

We define $e^t_{n,k} = (s^t_{n,k}, a^t_{n,k}, r^t_{n,k}, s^{t+1}_{n,k})$ as the experience sequence of agent (n,k) at time step t. The DQN is trained by the dataset $D = \{e^1_{1,1}, e^1_{1,2}, \ldots, e^t_{n,k} \cdots\}$, which describes the agents' relation with their environment. The key to using the DQN for solving (5) is to model the decision variables as the action of agents. Obviouly the normalized downlink transmission power $p_{n,k}$ is the decision variable for SE, therefore the action of agent (n,k) is $p_{n,k}$. We define $p^t_{n,k}$ as the action of agent (n,k) at time step t. The agent (n,k) takes action according to the current state $s^t_{n,k}$, which features the independent variables. From (4) we find that the large-scale fading is the independent variable for SE, therefore the large-scale fading matrix at time step t,

$$\boldsymbol{\beta}^t = \begin{bmatrix} \beta^t_{1,1} & \beta^t_{1,2} & \cdots & \beta^t_{1,K} \\ \beta^t_{2,1} & \beta^t_{2,2} & \cdots & \beta^t_{2,K} \\ \cdots & \cdots & \cdots & \cdots \\ \beta^t_{N,1} & \beta^t_{N,2} & \cdots & \beta^t_{N,K} \end{bmatrix} \tag{14}$$

is a key element for $s^t_{n,k}$. The objective function, which describes the target of the agents, is defined as the reward, i.e., the downlink sum-SE, achieved in each time step. Based on the above analysis, the elements of the experience etnk for CF mmWave massive MIMO power allocation are defined as following:

1) State $s^t_{n,k}$: The signal-to-interference-plus-noise ratio (SINR) is the key element of the SE. The signal in SINR of UE k comes from the agent set $\{(1,k), (2,k), \ldots, (N,k)\}$, while the interference in SINR for agent (n, k) mainly comes from the agent set $\{(n,1), (n,2), \ldots, (n,K)\}$. Therefore, for agent ($n$,

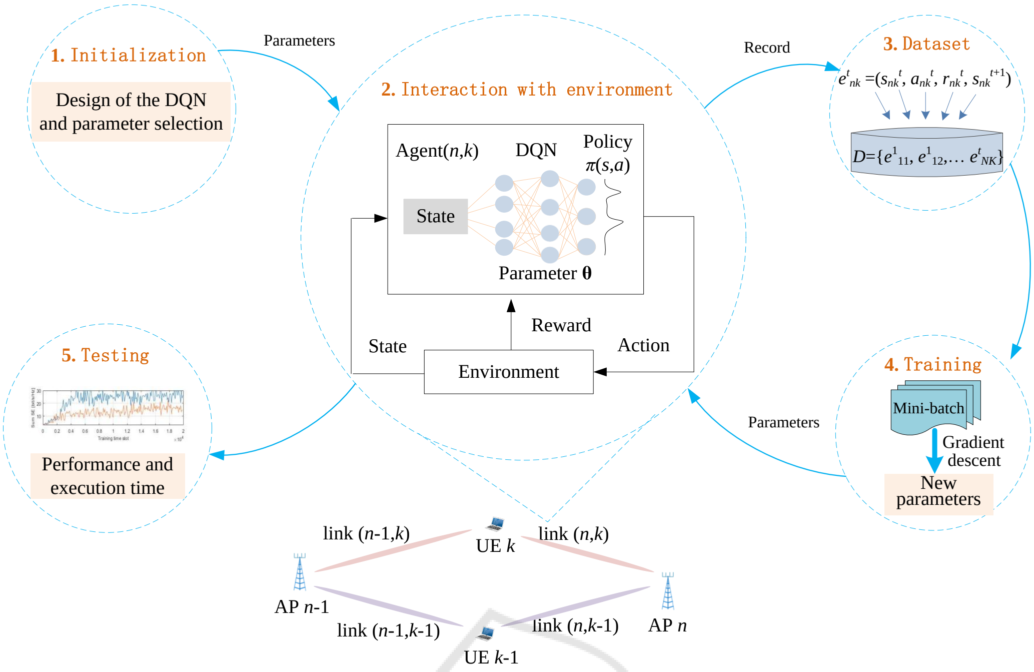

Figure 3: Illustration of the proposed multi-agent deep reinforcement learning system.

k) only the n-th row and k-th column of $\boldsymbol{\beta}^t$ are relevant. We normalize these elements by $\beta^t_{n,k}$ as data preprocessing. It has been determined experimentally that some auxiliary information can improve the sum-SE performance of DQN. Like in (Nasir and Guo, 2019) and (Meng and Chen, 2020), we consider two auxiliary information elements, namely the sum-SE $\sum_{k'=1}^{K} SE^{t-1}_{k'}$ and the power allocation $p^{t-1}_{n,k}$ at time step t-1. Finally, $s^t_{n,k}$ is formalized as follows:

$$s^t_{n,k} = \{\frac{\boldsymbol{\beta}^t(n,:)}{\beta^t_{n,k}}, \frac{\boldsymbol{\beta}^t(:,k)_{/\beta^t_{n,k}}}{\beta^t_{n,k}}, p^{t-1}_{n,k}, \sum_{k'=1}^{K} SE^{t-1}_{k'}\} \quad (15)$$

where $\boldsymbol{\beta}^t(n,:)$, $\boldsymbol{\beta}^t(:,k)$ represent the n-th row and k-th column of $\boldsymbol{\beta}^t$, respectively. The numerator of the second term in $s^t_{n,k}$ removes a redundant $\beta^t_{n,k}$. Therefore the size of $s^t_{n,k}$, i.e., the input dimension of the DQN, is $N+K+1$. One remark is that $\sum_{k'=1}^{K} SE^{t-1}_{k'}$ in (15) is the sum-SE at time step $t-1$. Each UE measures its SE and then sends it to the APs by the uplink at time step $t-1$. Then the CC collects this information as the input of the DQN at time step t. The process of sending SE values can be neglected in the power allocation process, since it occurs on the time scale of large-scale fading, similar to the $\boldsymbol{\beta}^t$ collection. In addition, compared to the $\boldsymbol{\beta}^t$ matrix (KNelements), there are only K elements of the SE information i.e., the SE of K UEs.

2) Action $a^t_{n,k}$: The allocated power is a continuous variable, however, for the action space of DQN, the dimension must be finite. Therefore we discretize the power as follows:

$$\boldsymbol{A} = \{0, \frac{p_{\max}}{|\boldsymbol{A}|-1}, \frac{2p_{\max}}{|\boldsymbol{A}|-1}, \dots, p_{\max}\} \quad (16)$$

where $|\boldsymbol{A}|$ represents the number of power levels.

3) Reward $r^t_{n,k}$: The target is to maximize the sum-SE. Therefore, the reward is the sum-SE at time step t:

$$r^t_{n,k} = \sum_{k=1}^{K} SE^t_k \quad (17)$$

3.3 Complexity of the Proposed DQN

The computational complexity considers the operational phase, i.e., the time period that a trained DQN performs the power allocation. Therefore the computational complexity of the DQN is only determined by the DNN. The computational complexity of a neural network depends on the number of neurons and layers. Specifically, for a fully-connected neural network, the complexity is O($\nu\mu^2$), where ν is the number of layers and μ is the number of neurons for the widest layer, i.e., the layer with the most neurons. Typically, the number of neurons in each layer depends on the dimension of the input layer, i.e., O(μ)=O($N+K+1$) in our case. The number of layers for a DQN is independent of the scale of the problem. Therefore the computational complexity of DQN is

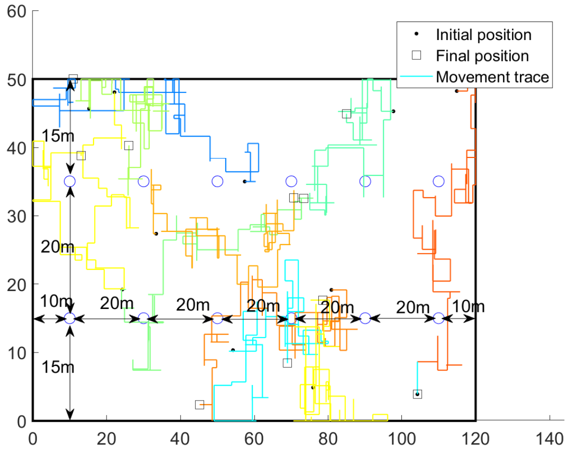

Figure 4: Example of UE movement traces in a 3GPP TR 38.901 scenario for 100 seconds.

O(N^2+K^2). Compared to the WMMSE algorithm O(IN^2K^3) in Section 2.4, the DQN has a much lower computational complexity.

4 SIMULATION RESULTS

In this section we show by simulations that the DQN-based power allocation in CF mmWave massive MIMO is competitive in terms of performance and complexity.

4.1 Scenario and Configuration

We consider the 3GPP TR 38.901 indoor mixed office scenario (120m×50m×3m) (3GPP, 2018) with 12 APs. Each AP contains 9 antennas in a horizontally mounted and downward radiating 3×3 UPA at a height of 3m. We assume K=10 single-antenna UEs moving within the coverage area. Each UE moves in a random direction (up, down, left, and right) with a randomly chosen velocity distributed uniformly between 0 and 1m/s. We consider a discrete time system where the duration of each time step is 0.2s, corresponding to the large-scale time (40 coherence times), as discussed in Section 3.2. The carrier frequency is 29 GHz, the bandwidth is 200 MHz. For a UE velocity of 1m/s, the channel coherence τ_c is about 5 ms, calculated as $\tau_c = \lambda/2v$, where λ is the wavelength and v is the velocity (Marzetta and Ngo.H.Q, 2016). Each UE maintains its speed and direction in each second before selecting a new speed and direction. The initial positions of the UEs at time t=0, are uniformly distributed over the coverage area (Fig.4). We model the large-scale fading as the combination of pathloss and shadowing, as in (3GPP, 2018).

Table 1: Parameters used in simulations.

Parameter	value
Coverage volume	120m×50m×3m
K, number of UEs	10
M, number of antennas per AP	9
N, number of APs	12
$p_{\max}$, maximum power constraint	13 dBm
p_p, pilot power	20 dBm
τ_c, length of coherence time in symbols	200
τ_p, length of pilot in symbols	5
Carrier frequency	29 GHz
Bandwidth	200 MHz
Noise power	-74dBm
Distribution of UE velocity	U(0, 1) m/s
Timeslot duration	0.2s

The maximum power constraint $p_{\max}$ is 13 dBm and the noise power is assumed to be -74 dBm. The uplink pilot power is 20 dBm. We set the coherence time to 200 modulation symbols as in (Q and Ashikhmin, 2017). We assume the length of the uplink pilot, used to determine the CSI, is 5 symbols. As discussed in (Q and Ashikhmin, 2017), when $\tau_p < K$ some pilot sequences are reused, hence the simulations take pilot contamination into consideration. The parameters used in the simulations are listed in Table I.

4.2 DQN Parameter Selection

We adopted a four-layer fully connected neural network, where the number of neurons in the two hidden layers are 128 and 64, respectively. This choice was based on what was proposed and worked well in (Nasir and Guo, 2019) and (Meng and Chen, 2020). We did not investigate whether different values for these hyperparameters would lead to better results. This may be a topic for further study. The number of neurons in the input layer is $N+K+1$ as discussed in (20), i.e., 22 in our case. We set the number of power levels equal to 10; therefore, the number of neurons in the output layer is 10.

It is worth pointing out that finding the best DQN parameters can be seen as an optimization problem in its own right. For a given problem, the training should be based on the particular network configuration and the usage scenarios to be expected. In this subsection we tried several parameters to find the best choice, i.e., those that give us the highest sum-SE during training. We studied the impact of the discount factor ω, the training interval C, the initial adaptive learning rate lr and the adaptive ε-greedy algorithm on the training of the DQN.

Adaptive learning means that the learning rate decays with the number of training time steps. Generally, a large learning rate allows the model to learn faster but may end up with a sub-optimal final set of weights. A smaller learning rate may allow the model to learn a more optimal or even globally optimal set of weights but may take significantly longer. Adaptive learning balances the training time and performance. The ε-greedy algorithm is a learning method that makes use of the exploration-exploitation tradeoff, in which the agent takes a random action (choosing a power level) with probability ε or takes the DQN output with probability 1-ε. A random action may lead the training 'jumps' out of a local optimum and explores new convergence regions. In the adaptive ε-greedy algorithm the value of ε decays each training time step. A large ε avoids the training ending up in local optima during the intial training time steps, a small value of ε makes sure that the training will converge in the later training time steps. Referring to the literatures, we choose $\omega \in \{0.1, 0.3, 0.5, 0.7, 0.9\}$(Meng.F and P., 2019), $C \in \{10, 50, 100, 200, 500\}$(Nasir and Guo, 2019; Mnih and Kavukcuoglu, 2013), $lr \in \{0.001, 0.005, 0.01, 0.05, 0.1\}$(Chien and Canh, 2020; Nasir and Guo, 2019), $\varepsilon \in \{0.1, 0.3, 0.5, 0.7, 0.9\}$(Mnih and Kavukcuoglu, 2013; Meng.F and P., 2019) to find the optimal configurations.

Fig.5 shows the effect of different parameters on the training process. The graphs on the left show the sum-SE as a function of time over a period of 20000 time steps. The corresponding graphs on the right show the empirical CDF of the sum-SE. In each of the figures we vary one parameter, while keeping the others constant.

Fig.5(a) shows the effect of the discount factor ω. Although the differences are not pronounced, we see that the sum-SE for ω=0.1 is always larger than for ω=0.9, by observing that the red line is to the right of the the blue line in the empirical CDF graph. The fluctuations of the sum-SE as a function of the training time, is due to the random mobility of the UEs, which leads to a variation of the large-scale fading.

Fig.5 (b) shows the effect of the training interval C. Similar observations can be found as in Fig.5(a), the differences between the lines are not pronounced. Nevertheless we find that C=100 achieves the highest sum-SE, by observing the light blue line in the empirical CDF graph.

Fig.5(c) shows the effect of the initial learning rate lr. The differences between the lines are not obvious, but we still see that the sum-SE for lr=0.005 achieves the highest sum-SE, by observing the light red line is to the right of other lines in the empirical CDF graph.

Fig. 5(d) shows the effect of ε-algortihm. We find that for different values of ε, the values of sum-SE are very different. It is obvious that ε=0.1 achieves the highest sum-SE, by observing the red line in both training process and empirical CDF graphs.

Based on the above observations, we choose the parameters ω=0.1, C=100, lr=0.005 and ε=0.1 to train the DQN. The length of the training period we choose is determined by the time it takes for the time-average of the sum-SE to converge to a stable value, i.e., a longer training period does not result in a significantly different time-average. In our case 30000 time steps, appears to be sufficiently long, as can be observed from Fig.6.

Observe that DQN achieves sum-SE values fluctuating around 23 bit/s/Hz around 5,000th training time steps. Afterward the average rises slowly and finally converges to around 30 bit/s/Hz after 20,000 training time steps. This is obviously better than the value obtained by the WMMSE algorithm, which is also shown in the figure as a reference benchmark. The random mobility of UEs causes the fluctuations of the sum-SE for both methods. It is clear that the DQN method, after sufficient training, achieves significantly better average sum-SE values than WMMSE.

4.3 Sum-SE Performance

We have used three benchmark algorithms to evaluate the performance of the DNQ based-power allocation. The first benchmark is the WMMSE algorithm described in Section 2.4, which is well-adopted and has been shown to perform well in cases studied in the literature (Sun and Chen, 2018; Nasir and Guo, 2019; Meng.F and P., 2019). The second benchmark is random power allocation where $p_{n,k} \sim U(0, p_{\max})$ for all n and k. The third one is full power allocation, i.e.,$p_{n,k} = p_{\max}$ for all n and k. We use the DQN that has been trained for 30000 time steps, as described in Fig.6 and run it for 1000 time steps. Fig.7 shows the sum-SE of the four methods over a period of 1000 time steps.

As expected, WMMSE and DQN have much better performance than random and full power allocation. In addition, the DQN method performs significantly better than WMMSE. The DQN method achieves around 10 bit/s/Hz higher sum-SE than the WMMSE algorithm.

4.4 Computational Complexity Comparison

To get an indication of the difference in computational complexity of DQN and WMMSE, we measured the

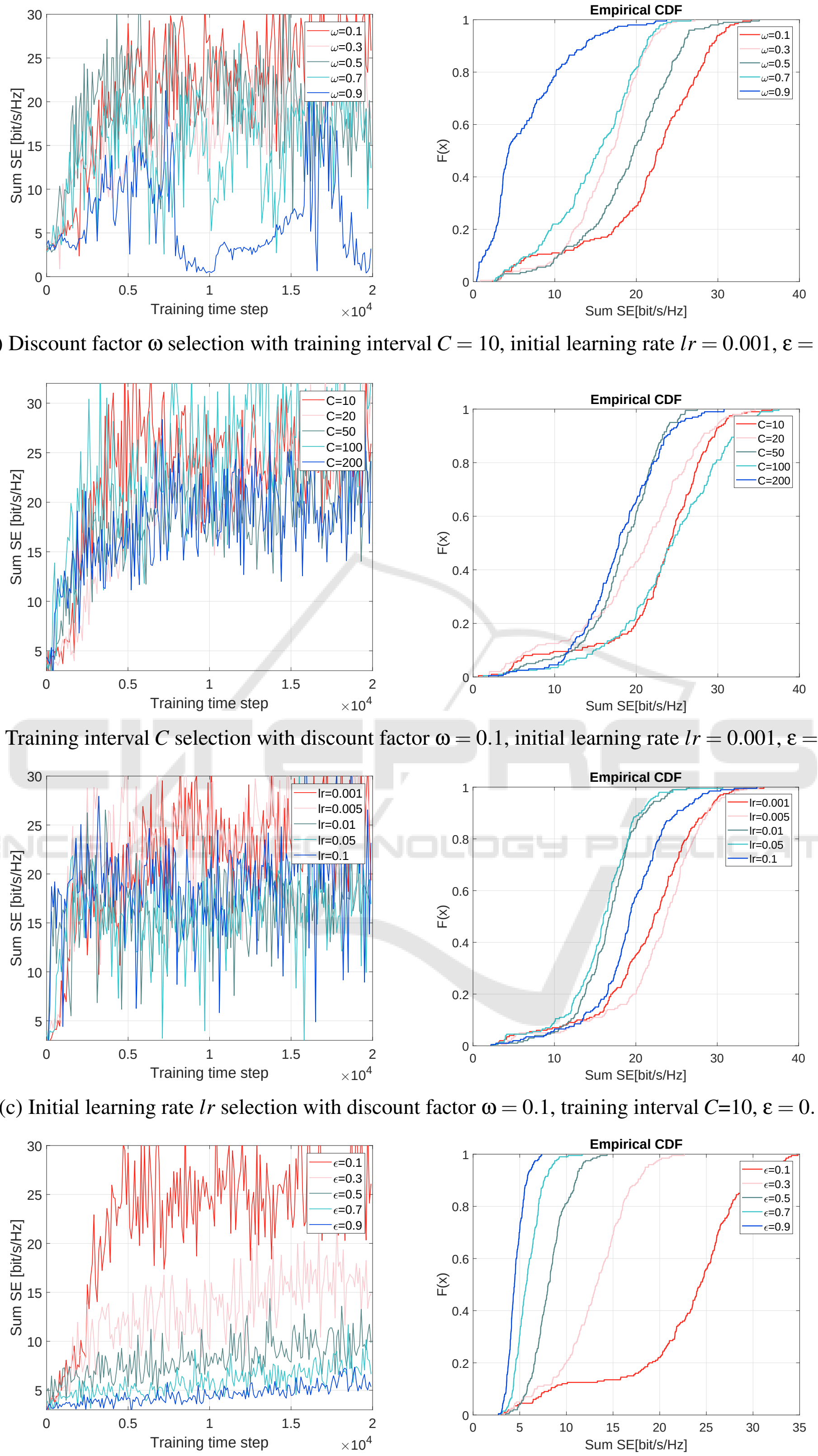

(a) Discount factor ω selection with training interval $C = 10$, initial learning rate $lr = 0.001$, $\varepsilon = 0.1$.

(b) Training interval C selection with discount factor $\omega = 0.1$, initial learning rate $lr = 0.001$, $\varepsilon = 0.1$.

(c) Initial learning rate lr selection with discount factor $\omega = 0.1$, training interval C=10, $\varepsilon = 0.1$.

(d) ε selection with discount factor $\omega = 0.1$, training interval C=10, initial learning rate $lr = 0.001$.

Figure 5: Effect of different parameters on the training process.

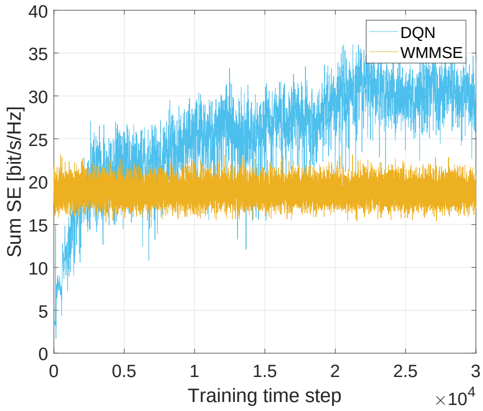

Figure 6: Training process of DQN with $\omega = 0.1, C = 100, lr = 0.005, \varepsilon = 0.1$.

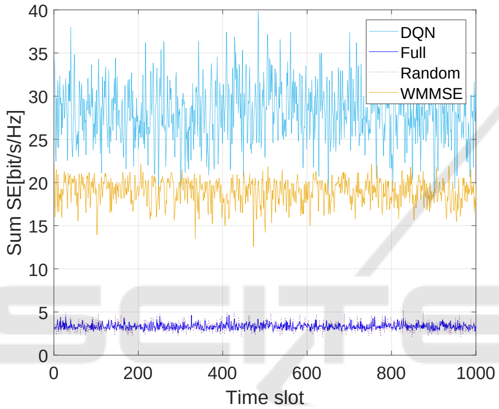

Figure 7: Comparison of sum-SE of DQN with the benchmark power allocation schemes over 1000 time steps, where DQN is trained with $\omega = 0.1, C = 100, lr = 0.005, \varepsilon = 0.1$.

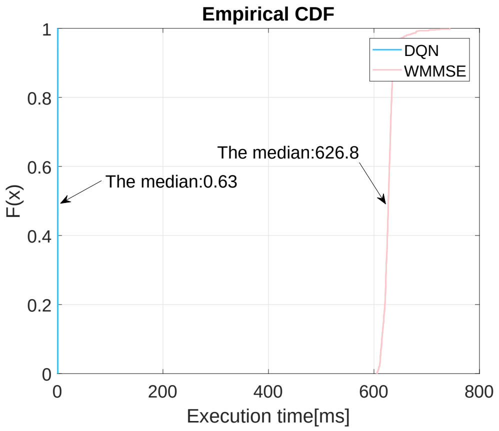

Figure 8: Execution time for DQN and WMMSE.

execution time in each of the 1000 time steps. We ran the algorithms on a 4 core Intel Core i5-7300 CPU with 2.6 GHz frequency. The programs are coded in Python 3.7.2 (DQN with Tensorflow 1.13.1). Fig.8 shows the empirical CDF of the execution times that we recorded for the two methods.

From Fig.8 it is obvious that DQN requires much less processing time than WMMSE and has less variation. It is around 0.6 ms for DQN while for WMMSE the execution time ranges from 600 ms to 750 ms. Recall that the power allocation is performed within each large-scale time, namely 0.2s in our case. It is obvious the DQN method meet this time constraint, while the WMMSE does not.

In addition, for DQN, the number of calculations is constant, as the number of neurons and layers does not change. Although it is invisible in Fig.8, there are still some slight fluctuations of execution time, which come from the calculation of different floating-point numbers and the inaccuracy of reading the system time. For WMMSE, the time fluctuation mainly comes from different initializations, i.e., a different initial point of the algorithm can make a large difference in the time needed to find the optimum. So we can conclude that the DQN method is expected to meet the requirements of real-time power allocation in a real implementation. One should note that the execution times shown in Fig.8 do not take into account the overhead for the information exchange between the APs and the CC via the fronthaul.

5 CONCLUSION

In this paper, we studied the use of DQN to allocate transmission power for maximizing the downlink sum-SE in CF mmWave massive MIMO systems with mobile UEs in an indoor scenario. Imperfect CSI and uplink pilot contamination were considered in the analysis. Unlike supervised learning that needs a huge dataset generated by other algorithms, the DQN is trained by interacting with the environment. The objective function, i.e., the sum-SE, is used as the reward to train the DQN. The sum-SE obtained by the DQN is significantly higher than the one achieved by the well-adopted WMMSE algorithm. In addition, the time-complexity of the DQN method is very low. The numerical results show that the DQN is expected to satisfy the stringent time constraints of power allocation in CF mmWave massive MIMO. There are still open issues to be addressed:

1. Online learning, which is expected to be processed in the real deployment of DQN, should be further studied to accommodate the scenarios with real measurements of channels and mobility of real UEs.

2. Different power allocation objective function, e.g., max-min policy, should be studied.

3. We assumed a Markovian UE mobility model. The mobility of real UEs is non-Markovian, which

might lead to an inefficient training of the DQN. This should be further investigated.

4. When, during operation, significant changes in the network configuration, e.g., the number of active APs, or in the temporal and spatial traffic characteristics, occur, the DQN should be retrained. When that should happen and what impact it would have on the operation of the system has not been addressed yet and requires further study.

5. For the hyper-parameters of the DQN, i.e., the number of layers and neurons, we used values taken from the literature. One could investigate whether these hyper parameters could be optimized to get better results in terms of the achieved sum-SE.

REFERENCES

3GPP (2018). Study on channel model for frequencies from 0.5 to 100 GHz (Release 15). In *IEEE 21st International Workshop on Computer Aided Modelling and Design of Communication Links and Networks*. 3GPP.

Alkhateeb, A. and Mo, J. (2014). MIMO precoding and combining solutions for millimeter-wave systems. In *IEEE Communications Magazine*. IEEE.

Alonzo, M. and Buzzi, S. (2019). Energy-efficient power control in cell-free and user-centric massive MIMO at millimeter wave. In *IEEE Transactions on Green Communications and Networking*. IEEE.

Andrews and G., J. (2014). What will 5G be? In *IEEE Journal on Selected Areas in Communications*. IEEE.

Björnson, E. and Hoydis, J. (2017). *Massive MIMO Networks: Spectral, Energy, and Hardware Efficiency*. Foundations and Trends in Signal Processing, Hanover.

Busari, S. A. and Huq, K. M. S. (2018). Millimeter-wave massive MIMO communication for future wireless systems: A survey. In *IEEE Communications Surveys & Tutorials*. IEEE.

C, G. and K, H. (2013). On mm-wave multipath clustering and channel modeling. In *IEEE Transactions on Antennas and Propagation*. IEEE.

Chen, Z. and Björnson, E. (2018). Channel hardening and favorable propagation in cell-free massive MIMO with stochastic geometry. In *IEEE Transactions on Communications*. IEEE.

Chien, T. V. and Canh, T. N. (2020). Power control in cellular massive MIMO with varying user activity: A deep learning solution. In *IEEE Transactions on Wireless Communications*. IEEE.

F, S. and W., Y. (2016). Hybrid digital and analog beamforming design for large-scale antenna arrays. In *IEEE Journal of Selected Topics in Signal Processing*. IEEE.

González-Coma, J. P. and Rodríguez-Fernández, J. (2018). Channel estimation and hybrid precoding for frequency selective multiuser mmWave MIMO systems. In *IEEE Journal of Selected Topics in Signal Processing*. IEEE.

Hamdi, R. and Driouch, E. (2016). Resource allocation in downlink large-scale MIMO systems. In *IEEE Access*. IEEE.

I, A. and H, K. (2018). A survey on hybrid beamforming techniques in 5G: Architecture and system model perspectives. In *IEEE Communications Surveys & Tutorials*. IEEE.

Interdonato, G. and Ngo, H. Q. (2016). On the performance of cell-free massive MIMO with short-term power constraints. In *IEEE 21st International Workshop on Computer Aided Modelling and Design of Communication Links and Networks*. IEEE.

Larsson, E. G. and Edfors, O. (2014). Massive MIMO for next generation wireless systems. In *IEEE Communications Magazine*. IEEE.

LeCun and Bengio (2015). Deep learning. In *Nature*. Nature.

Lin and Cong, J. (2019). Hybrid beamforming for millimeter wave systems using the MMSE criterion. In *IEEE Transactions on Communications*. IEEE.

M, L. and T., Z. (2014). Efficient mini-batch training for stochastic optimization. In *Proceedings of the 20th ACM SIGKDD international conference on Knowledge discovery and data mining*. ACM.

Mai, T. C. and Ngo, H. Q. (2020). Downlink spectral efficiency of cell-free massive MIMO systems with multi-antenna users. In *IEEE Transactions on Communications*. IEEE.

Marzetta and Ngo.H.Q (2016). *Fundamentals of massive MIMO*. Cambridge University Press, Cambridge.

Meng, F. and Chen, P. (2020). Power allocation in multi-user cellular networks: Deep reinforcement learning approaches. In *IEEE Transactions on Wireless Communications*. IEEE.

Meng.F and P., C. (2019). Power allocation in multi-user cellular networks with deep Q learning approach. In *IEEE International Conference on Communications*. IEEE.

Mnih and Kavukcuoglu (2013). Human-level control through deep reinforcement learning. In *Nature*. Nature.

N, B. E. and H, I. (1989). The Bellman equation for minimizing the maximum cost. In *Nonlinear Analysis: Theory, Methods & Applications*.

Nasir, Y. S. and Guo, D. (2019). Multi-agent deep reinforcement learning for dynamic power allocation in wireless networks. In *IEEE Journal on Selected Areas in Communications*. IEEE.

Nikbakht, R. and Jonsson, A. (2019). Unsupervised-learning power control for cell-free wireless systems. In *IEEE 30th Annual International Symposium on Personal, Indoor and Mobile Radio Communications*. IEEE.

O., E. A. and S., R. (2014). Spatially sparse precoding in millimeter wave MIMO systems. In *IEEE transactions on wireless communications*. IEEE.

Polegre, A. . and Palou, F. R. (2020). New insights on channel hardening in cell-free massive MIMO networks. In

2020 IEEE International Conference on Communications Workshops. IEEE.

Q, N. H. and Ashikhmin (2017). Cell-free massive MIMO versus small cells. In *IEEE Transactions on Wireless Communications*. IEEE.

Shi, Q. and Razaviyayn, M. (2011). An iteratively weighted MMSE approach to distributed sum-utility maximization for a MIMO interfering broadcast channel. In *IEEE Transactions on Signal Processing*. IEEE.

Sun, H. and Chen, X. (2018). Learning to optimize: Training deep neural networks for interference management. In *IEEE Transactions on Signal Processing*. IEEE.

Yu, X. and Shen, J. (2016). Alternating minimization algorithms for hybrid precoding in millimeter Wave MIMO systems. In *IEEE Journal of Selected Topics in Signal Processing*. IEEE.